Acta Scientiarum
http://periodicos.uem.br/ojs
ISSN on-line: 1807-8664
https://doi.org/10.4025/actascitechnol.v48i1.71579
CC BY

Dynamics and control of an energy harvesting system using the Lyapunov-Floquet transformation and sensitivity analysis using Sobol indices

Luiz Oreste Cauz[1,2*], Fábio Roberto Chavarette[2], Lakshmi Narayan Mishra[3] and Laxmi Rathour[4]

[1]Universidade Estadual de Mato Grosso do Sul, Rua Valter Hubacher, 138, Vila Beatriz, 79750-000, Nova Andradina, Mato Grosso do Sul, Brazil. [2]Faculdade de Engenharia, Universidade Estadual Paulista, Ilha Solteira, São Paulo, Brazil. [3]Department of Mathematics, School of Advanced Sciences, Vellore Institute of Technology, Tamil Nadu, India. [4]Department of Mathematics, National Institute of Technology, Mizoram, India. *Author for correspondence. E-mail: luiz.cauz@unesp.br

ABSTRACT. This study aimed to design a linear feedback control approach for a parametrically excited energy harvesting system utilizing a piezoelectric material as the transduction element. The purpose was to significantly increase the amount of energy produced compared to that produced by the original system. To do so, firstly, it is necessary to analyze the stability of the system and perform a global sensitivity analysis to determine the physical parameters of the system that most contribute to energy production. The sensitivity analysis is done by calculating the Sobol indices, which are statistical indices that measure the relative contribution of each input variable (in this case, the physical parameters of the system) to the contribution of all input variables. In the stability analysis, the state transition matrix approximation techniques created by Sinha and Butcher and the results of the Floquet Theory for periodic systems were used. Stability analysis and global sensitivity analysis are methodologically complementary techniques for a better understanding of the dynamics of a system. In the case of this work, they are applied to an energy-harvesting system based on mechanical vibrations, providing important information to design a more efficient controller. The control technique used was proposed by Sinha and Butcher (1997), and is known as Linear Feedback Controller Design via the Lyapunov-Floquet Transform.

Keywords: Stability analysis; global sensitivity analysis; lyapunov-floquet transformation; linear feedback control.

Received on March 08, 2024.
Accepted on June 11, 2025.

Introduction

The process of energy harvesting involves converting ambient energy into a functional and usable form. Among the most commonly exploited sources for such devices are solar energy, thermal gradients, and acoustic and mechanical vibrations (Andò et al., 2010). When implementing new technologies, it is necessary to research and develop devices capable of producing the energy needed for these technologies to be self-sufficient, i.e., capable of producing enough energy for their consumption. Mechanical vibrations are one way of obtaining energy from the environment. Vibration Energy Harvesting Systems (VEHS) harness mechanical vibrations as their primary energy source. Although VEHS generate relatively small amounts of power, they remain essential since many devices require minimal energy. Vibration energy harvesting, often considered supplemental power, can supply energy for low-load applications or sustain remote devices and sensors that demand limited power. Examples include hearing aids, pacemakers, spinal cord stimulators, and microelectromechanical systems. The high cost and invasiveness of procedures needed to replace pacemaker batteries present significant challenges, while spinal cord stimulators require frequent recharging, which can be both painful and time-consuming. Ideally, these devices would incorporate energy harvesting systems to enable self-recharging and continuous operation over their lifespan. Research on implementing VEHS within the human body has shown promising results, with initial studies indicating that blood vessel contractions could generate up to 20 mW of energy per day (Sohn et al., 2005). Many studies have focused on Vibration Energy Harvesting Systems (VEHS), especially those using piezoelectric materials as transducers that convert mechanical energy into electrical energy. Lead Zirconate Titanate (PZT) is among the most commonly used piezoelectric materials (Challa et al., 2008; Eichhorn et al., 2009; Zhu, 2011).

Several uncertain factors influence the electrical energy output of such systems, including the amplitude, frequency, and physical characteristics of the excitation force. Studies addressing issues of imprecision and

uncertainty in parameters are increasingly common, as we can see in Sharma et al. (2023) and Rathour et al (2024); however, most research on applied dynamics does not address the uncertainty and variation of the system's parameters, that is, no criteria are defined to determine which parameters exert the greatest influence on system behavior. One possible approach to this problem is global sensitivity analysis (Cacuci, 2003), which is a computationally efficient technique based on statistical methods that use Sobol indices, which are variance-based measures that quantify the contribution of input parameters to portions of an expansion polynomial. Statistical methods are widely used in research into applied dynamics problems, as observed in Outa et al (2021).

In the stability analysis, the Lyapunov-Floquet (L-F) method is employed, utilizing Chebyshev polynomial expansion to approximate periodic components. The state transition matrix is approximated through the Picard iterative method. This approach enables the determination of Floquet multipliers and facilitates the construction of the dynamic system's stability diagram.

Stability analysis and global sensitivity analysis are complementary and robust tools for investigating the dynamic behavior of the system. Stability analysis enables the assessment of system stability by examining the influence of periodic terms inherent to the governing equations. In contrast, global sensitivity analysis identifies the physical parameters that most significantly influence the system's ability to achieve a desired performance. In the present study, the focus lies on identifying periodic solutions through stability analysis and determining the parameter configurations that maximize energy output through global sensitivity analysis.

The two aforementioned techniques provide critical insights that can inform the development of more effective control strategies aimed at enhancing energy harvesting performance. The control methodology adopted in this study builds upon the foundational works of Sinha and Joseph (1994), David and Sinha (2000), and Sinha and Dávid (2006).

Material and methods

The methodology used here is primarily based on techniques that complement each other, for a more accurate analysis of the dynamics of periodic time-varying systems, namely, Stability Analysis via Lyapunov-Floque Transformation and Global Sensitivity Analysis. The stability analysis method adopted in this study was originally developed by Sinha and Butcher (1997). For the global sensitivity analysis, a variance-based method employing the computation of Sobol indices was adopted, as described in Cauz et al (2023), Soize (2017), and Cacuci (2003). These two techniques can be integrated in a complementary way, establishing a two-way analysis framework that provides a comprehensive view of the system's dynamic behavior. This information is essential for guiding the development of more effective control strategies. Figure 1 shows a schematic representation of the methodologies applied.

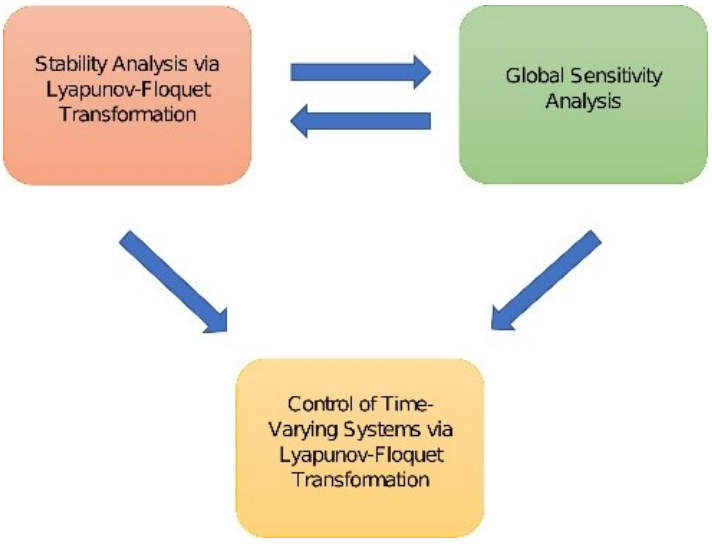

Figure 1. Schematic representation of the Methodology.

Global sensitivity analysis

In general, mathematical models that represent physical phenomena have input parameters whose impact on the dynamic behavior of the system is not known a priori. Moreover, in many models, some parameters

affect the response of the system more than others. The global sensitivity analysis seeks to quantitatively determine the influence of each input parameter on the variability of the system response. As a result of this analysis, it is possible to x the nominal values of some parameters, varying only the values of the most relevant parameters. The analysis method adopted herein is based on the Hoeffding-Sobol decomposition and aims to establish an approximation of the original model by a computational model in sums of increasing dimensionality, subsequently allowing one to evaluate the variance of each of the terms about the total variance of the model.

Suppose the mathematical model is represented by the following functional relationship

$$\mathrm{Y} = \mathcal{M}(\mathrm{X}), \mathrm{X} = \{\mathrm{X}_1, \mathrm{X}_2, \dots, \mathrm{X}_n\}$$

where X is a vector of independent parameters that are modified by the mathematical operator $\mathcal{M}$, producing a scalar output Y. The Hoeffding-Sobol decomposition is written as the sum of terms of different dimensions

$$\mathrm{Y} = \mathcal{M}_0 + \sum_{i=1}^{n} \mathcal{M}_i(\mathrm{X}_i) + \sum_{\mathrm{i<j}} \mathcal{M}_{ij}(\mathrm{X}_i, \mathrm{X}_j) + \cdots + \mathcal{M}_{1,\dots,n}(\mathrm{X}_1, \mathrm{X}_2, \dots, \mathrm{X}_n),$$

where $\mathcal{M}_0 = \mathrm{E}[\mathrm{Y}]$, $\mathcal{M}_i = \mathrm{E}[\mathrm{Y}|\mathrm{X}_i] - \mathcal{M}_0, \mathcal{M}_{ij} = \mathrm{E}\left[\mathrm{Y}\middle|\mathrm{X}_i, \mathrm{X}_j\right] - \mathcal{M}_0 - \mathcal{M}_i(\mathrm{X}_i) - \mathcal{M}_j(\mathrm{X}_j)$ and so on. The operator $\mathrm{E}[\cdot]$ denotes the expected value of the quantity to be calculated.

From the independence of the parameters of X, the global variance of Y is written as

$$\mathrm{Var}[\mathrm{Y}] = \sum_u \mathrm{Var}[\mathcal{M}_u(\mathrm{X}_u)],$$

with $\sum_u \mathrm{Var}[\mathcal{M}_u(\mathrm{X}_u)] = \sum_{i=1}^{n} \mathrm{Var}\,[\mathcal{M}_i(\mathrm{X}_i)] + \sum_{\mathrm{i<j}} \mathrm{Var}\,[\mathcal{M}_{ij}(\mathrm{X}_i, \mathrm{X}_j)] + \cdots + \mathrm{Var}\,[\mathcal{M}_{1,\dots,n}(\mathrm{X}_1, \mathrm{X}_2, \dots, \mathrm{X}_n)]$
and therefore,

$$\sum_u \frac{\mathrm{Var}[\mathcal{M}_u(\mathrm{X}_u)]}{\mathrm{Var}[\mathrm{Y}]} = \sum_u \mathrm{S}_u = \sum_{i=1}^{n} \mathrm{S}_i + \sum_{i<j} \mathrm{S}_{ij} + \cdots + \mathrm{S}_{1,2,\dots,n} = 1 \quad (1)$$

where S_u is known as Sobol indices. Each Sobol index represents the contribution of the variance of the output of X_u to the total variance of the output.

The first-order Sobol indices

$$\mathrm{S}_i = \frac{\mathrm{Var}[\mathcal{M}_i(\mathrm{X}_i)]}{\mathrm{Var}[\mathrm{Y}]}$$

describes the individual effect of X_i, while the second-order indices

$$\mathrm{S}_{ij} = \frac{\mathrm{Var}[\mathcal{M}_{ij}(\mathrm{X}_i, \mathrm{X}_j)]}{\mathrm{Var}[\mathrm{Y}]}$$

measure the joint contribution of the pair $(\mathrm{X}_i, \mathrm{X}_j)$, and so on.

Polynomial chaos expansion

The Monte Carlo Method is used in applied dynamics problems to evaluate uncertainty and variability in systems, through stochastic simulation of different scenarios, as can be seen in Sharma et al (2022), who used Monte Carlo Simulation for decision-making in medical diagnostic processes in an uncertain environment. The Monte Carlo method is one way to calculate Sobol indices. Due to the slow convergence of this sampling method, the use of this method may not be computationally interesting. An alternative and effective way to calculate Sobol indices is to use a surrogate model of the original model. This method is obtained through the Polynomial Chaos Expansion (PCE) (Soize, 2017), which approximates the original physical system and allows calculations to have a high accuracy with little computational processing. In short, PCE is a way to approximate solutions to the original system. In the literature, there are several methods and research that involve polynomial approximations, such as the Lagrange polynomial method (Bhat et al., 2024).

Suppose $\mathrm{Y} = \mathcal{M}(\mathrm{X})$ is a random variable of finite variance. One can then define a Polynomial Chaos Expansion in the form

$$\mathrm{Y} \approx \sum_{\alpha \in A} y_\alpha \Psi_\alpha(\mathrm{X})$$

Where Ψ_α are orthogonal polynomials of several variables with respect to a joint probability density function f_X of X; y_α are real coefficients to be determined, and $A \subset N^M$ such that it is possible to select all possible indices of the polynomial expansion.

Because of the orthogonality of a PCE, we have $\mathrm{E}[\mathrm{Y}] \approx y_0$ and

$$\mathrm{Var}[\mathrm{Y}] \approx \sum_{\substack{\alpha \neq 0 \\ \alpha \in A}} y_\alpha^2 \quad (2)$$

From Eq. (2) and the definition of the Sobol index (Eq. (1)), we can rewrite the first and second-order Sobol indices, respectively, as

$$S_i = \left(\sum_{\alpha\neq 0,\ \alpha\in A_i} y_\alpha^2\right)\Big/\left(\sum_{\alpha\neq 0,\ \alpha\in A} y_\alpha^2\right),\ S_{ij} = \left(\sum_{\alpha\neq 0,\ \alpha\in A_{ij}} y_\alpha^2\right)\Big/\left(\sum_{\alpha\neq 0,\ \alpha\in A} y_\alpha^2\right).$$

Thus, the Sobol indices can be written in terms of the coefficients y_α of the Polynomial Chaos Expansion. These coefficients can be computed by numerical methods, such as the projection method and the regression method (Soize, 2017).

Stability analysis

In the analysis of system stability (Eq. (25)), we employ Floquet theory, originally formulated by the French mathematician Gaston Floquet (1847–1920), in conjunction with a methodology proposed by Sinha and Butcher (1997). Floquet theory is particularly well-suited for analyzing the stability of periodic orbits when the analytical form of the corresponding solutions is known (Meirovitch, 2010; Monteiro, 2011; Naifeh & Balachandra, 1995). More precisely, Floquet demonstrated that, under certain regularity conditions, the stability analysis of linear time-periodic systems can be reduced to the study of an equivalent linear time-invariant system via a coordinate transformation. Nevertheless, the direct analytical application of Floquet theory is limited in practice due to the complexity of obtaining closed-form solutions for general periodic systems.

The method proposed by Sinha and Butcher combines Picard iterations with Chebyshev polynomial expansions to obtain approximate solutions for linear time-periodic systems (Andrade et al., 2012). A comprehensive formulation and analysis of this technique are presented in Sinha and Butcher (1997).

The main formulation and theorems of the Lyapunov-Floquet Theory are presented below.

Some results from the lyapunov-floquet theory

Consider a system of n first-order linear differential equations expressed as

$$\dot{x}(t) = A(t)x(t) \tag{3}$$

where $x(t) \in \mathbb{R}^n$, $A(t) \in \mathbb{R}^{n\times n}$. The matrix A has elements $A_{ij}(t)$ that are continuous and periodic in time with period T, such that $A(t+T) = A(t)$ for all $t \geq 0$. Thus, this system (Eq. 2.3) is said to be periodic in time. Suppose the system (Eq. 3) admits n linearly independent solutions $x^{(j)}(t)$. These solutions constitute a fundamental set, allowing any general solution of the system to be expressed as a linear combination of them. This set of solutions can be represented in matrix form as $\Phi(t)$, referred to as the fundamental matrix solution or state transition matrix (STM) of the system

$$\Phi(t) = \left[x^{(1)}(t)\ x^{(2)}(t)\ \cdots\ x^{(n)}(t)\right].$$

In 1883, Floquet proposed the following result (Meirovitch, 1970):

Theorem 1. If $\Phi(t)$ is an STM of the system described by Eq. 3 where $A(t+T) = A(t)$ for all $t \geq 0$, then $\Phi(t+T)$ is also an STM of the system (Eq. 3). Moreover, for each STM Φ(t) there exists a non-singular periodic matrix $Q(t)$ of periodic T (with $Q(0) = I$) and a constant matrix R, such that

$$\Phi(t) = Q(t)e^{Rt}. \tag{4}$$

More specifically, if R is a real (or complex) matrix of constant coefficients, then $Q(t)$ is $2T$ periodic (or T periodic) (Iakubovich & Starzinskii, 1975). From (Eq. 4), it can be seen that the decay of the system is determined by the term e^{Rt} and, in the case, when $t = T$, the R matrix can be calculated by

$\Phi(T) = e^{RT}$

where the matrix $\Phi(t)$ is calculated at the end of period T. The matrix $\Phi(T)$ is called the Floquet Transition Matrix (*FTM*), also known as the Monodromy Matrix, and its eigenvalues ρ_j are called characteristic multipliers or Floquet multipliers (Monteiro, 2011). The R matrix is obtained from the *FTM* matrix using the identity (Sinha et al., 2000):

$$R = \frac{1}{2T}\log\Phi(2T) = \frac{1}{2T}\log[\Phi(T)]^2.$$

By Theorem 1, and by applying a coordinate transformation known as the Lyapunov-Floquet transformation (or simply the L-F transformation), we obtain the following corollary:

Corollary 1. The Lyapunov-Floquet transformation, T-periodic

$x(t) = Q(t)z(t)$

with $z(t) \in \mathbb{R}^n$, $Q(t+T) = Q(t), Q(0) = I_n$, in which I_n is the identity matrix of order n, transforms the time-variant system $\dot{x}(t) = A(t)x(t)$, in the time-invariant system $\dot{z}(t) = Rz(t)$, where the eigenvalues λ_j of R are related to the characteristic multipliers by means of

$$\rho_j = e^{\lambda_j T}. \tag{5}$$

It can be concluded from Eq. (5) that the characteristic exponents are given as follows (Sharma & Sinha, 2018):

$$\lambda_j = \frac{1}{T}\left(\log|\rho_j| + i \arg \rho_j\right), j = 1,2,\cdots,n. \tag{6}$$

Remark 1. Note from Corollary 1 that a linear system with periodic coefficients (time-invariant) can be transformed into a linear system with constant coefficients (time-invariant).

The numbers λ_j are called characteristic exponents or Floquet exponents. The stability of the system (Eq. 3) can be studied by analyzing the characteristic exponents, as can be seen from the following theorem (Meirovitch, 2010):

Theorem 2. About the stability of the system (Eq. 3), we have the following results:

i) If all characteristic exponents have the negative real part, then all solutions of the system (Eq. 3) are asymptotically stable.

ii) If at least one of the characteristic exponents has the positive real part, then the system (Eq. 3) is unstable.

iii) If all characteristic exponents have zero or negative real parts, and those with zero real parts are simple roots of the characteristic polynomial of R, then the system is stable; if the roots with zero real parts are not simple, then the system is unstable.

Because of Eq. (6) and Theorem 2, the asymptotic stability of the system (Eq. 3) related to the Floquet multipliers is given in terms of the following corollary:

Corollary 2. If $|\rho_j| < 1$, for all $j = 1,2,\cdots,n$, then the system (Eq. 3) is asymptotically stable. If $|\rho_j| > 1$ for some j, the system is unstable.

Sinha and Butcher's technique for state transition matrix approximation

The great difficulty in applying both Theorems 1 and 2 is in obtaining the State Transition Matrix (STM) $\Phi(t)$. This difficulty is overcome when the theorems are applied to commutative systems. However, in most cases, it is practically impossible to obtain the matrix STM $\Phi(t)$. To circumvent this problem, Sinha and Butcher (1997) developed a numerical computational method to approximate the STM $\Phi(t)$.

Consider a nonlinear periodic dynamical system of dimension n of the form

$$\dot{z}(t) = f(z(t), t, \alpha) = f(z(t), t+T, \alpha), z(0) = z^0 \tag{7}$$

where $t \in \mathbb{R}^+$ denotes time, $z \in \mathbb{R}^n$ is the state vector, $\alpha \in \mathbb{R}^m$ is a vector of system parameters, and $f: \mathbb{R}^n \times \mathbb{R}^+ \times \mathbb{R}^m \to \mathbb{R}^n$ is analytic in the z and α components and periodic of period T at time t. Suppose that $\bar{z}$ is an equilibrium or periodic solution of period KT of the system (Eq. 7) and $x(t) = z(t) - \bar{z}(t)$ a perturbation of this solution. Thus, by expanding in Taylor series the system (Eq. 7) around $z = \bar{z}$, we have

$$\dot{x} = A(t,\alpha)x + f_2(x,t,\alpha) + f_3(x,t,\alpha) + \cdots + f_r(x,t,\alpha) + O(|x|^{r+1}), x(0) = x^0 = z^0 - \bar{z}(0) \tag{8}$$

where f_r represents the terms of order r ($r \geq 2$) of the Taylor series expansion of f, and $A(t,\alpha)$ and $f_r(x,t,\alpha)$ are periodic of period KT. Consider the linear part of Eq. (8) given by

$$\dot{x}(t,\alpha) = A(t,\alpha)x(t,\alpha), x(0,\alpha) = x^0. \tag{9}$$

Considering Eqs. (3) and (9) and theorem 1, the local stability of Eq. (8) is given by the Floquet multipliers ρ_j of the Floquet transition matrix (*FTM*) $\Phi(KT,\alpha)$.

To introduce the Sinha and Butcher technique, we change the variable $t = KT\tau$ to transform the linear system (Eq. (9)) of period KT into the following system of period 1

$$\frac{d}{d\tau}x(\tau,\alpha) = \bar{A}(\tau,\alpha)x(\tau,\alpha), \bar{A}(\tau+1,\alpha) = \bar{A}(\tau,\alpha), x(0,\alpha) = x^0, \tag{10}$$

where

$$\bar{A}(\tau,\alpha) = \bar{A}_1(\alpha)f_1(\tau) + \bar{A}_2(\alpha)f_2(\tau) + \cdots + \bar{A}_r(\alpha)f_r(\tau), \bar{A}_i(\alpha) = TA_i(\alpha), i = 1,2,\cdots,r.$$

According to Sinha and Butcher (1997) and Butcher and Sinha (1998), the state transition matrix (STM) $\Phi(\tau, \alpha)$ of the system (Eq. 10) can be approximated by

$$\Phi^{(p,m)}(\tau, \alpha) = \hat{T}^T(\tau)\left[\hat{I} + \left(\sum_{k=1}^{p-1}[L(\alpha)]^{k-1}\right)P(\alpha)\right].$$

where in the (p, m), p is the number of Picard iterations, m is the number of terms of modified Chebyshev polynomials $T_1^*(t), T_2^*(t), \cdots, T_{m-1}^*(t)$, $\hat{T}^T$ is the Chebyshev polynomial matrix, $L(\alpha) = \hat{G}^T\hat{Q}_D$, and $P(\alpha) = \hat{G}^T D(\alpha)$. Sinha and Butcher (1997) describe the process for constructing the $D(\alpha)$ matrix and obtaining the operational matrices $\hat{I}$, $\hat{G}$, and $\hat{Q}_D$.

Control of periodic systems via lyapunov-floquet transformations

Based on the techniques of Sinha and Butcher (1997), Sinha and Joseph (1994), and Sinha and Dávid (2006), the control method based on Lyapunov-Floquet transformations is described.

Consider the time-invarying nonlinear system represented by

$$\dot{x} = f(x(t), t) + u_c(t), \tag{11}$$

in which $x(t) \in \mathbb{R}^n$, which exhibits a chaotic attractor for a given set of parameters when $u_c(t) = 0$, and let $y(t)$ be the desired reference trajectory and $x(t)$ the trajectory of the controlled system. The goal of the control law u_c is to control the chaotic dynamics of the system so that $x(t)$ converges to $y(t)$. To this end, the control input $u_c(t)$ is structured into two distinct components

$$u_c(t) = u_f + u_t, u_f = \dot{y} - f(y(t), t), u_t = F(t)u(t).$$

The u_f part of the controller is called feedforward, and the u_t part is feedback. The matrix $F(t)$ is called the gain matrix and will be obtained next.

We can then rewrite the system (Eq. 11) in the form

$$\dot{x} = f(x(t), t) + \dot{y} - f(y(t), t) + F(t)u(t).$$

By defining $e(t) = x(t) - y(t)$ as the dynamic error between $x(t)$ and $y(t)$, it follows that

$$\dot{e} = g(e(t), t) + F(t)u(t), \tag{12}$$

where $g(e(t), t) = f(e(t) + y(t), t) - f(y(t), t)$ is a nonlinear function of class C^1.

If the following condition is satisfied

$$\lim_{\|e\|\to 0} \sup_{t\geq 0} \frac{\|g(e, t) - A(t)e + F(t)u(t)\|}{\|e\|} = 0,$$

where $A(t) \in \mathbb{R}^{n\times n}$ and

$$A(t) = \left[\frac{\partial g_j}{\partial e_i}\right]_{(0,t)},$$

one can then linearize (12) in the neighborhood of $e = 0$ and obtain

$$\dot{e} = A(t)e(t) + F(t)u(t). \tag{13}$$

Now, consider that the system described in Eq. (13) can be expressed in the general form

$$\dot{z} = A(t)z(t) + B(t)u_t, \tag{14}$$

in which the matrices $A(t)$ and $B(t)$ are periodic with period T and the pair $[A, B]$ is controllable. Using the Lyapunov-Floquet transformation (Sinha & Butcher, 1997)

$z(t) = Q(t)q(t)$,

in Eq. (14), we get

$$\dot{q} = Rq(t) + Q^{-1}(t)B(t)u_t, \tag{15}$$

in which $R = \frac{1}{2T}\ln(\Phi^2(T))$ and $\Phi(T)$ is the Floquet transition matrix.

Since the gain matrix $Q^{-1}(t)B(t)$ of the system (Eq. 15) is invariant in time, the aim is to build an auxiliary system with a gain matrix that remains constant over time

$$\dot{\bar{q}} = R\bar{q} + B_0 v(t), \tag{16}$$

where B_0 is a constant matrix of full rank such that the pair $[R, B_0]$ is controllable. Consider the control law v given by

$$v(t) = F_0\bar{q}(t), \tag{17}$$

in which F_0 denotes the gain matrix associated with the control input $v(t)$ which is designed to ensure that the system described by Eq. (17) is asymptotically stable.

If we define the dynamic error as $\varepsilon(t) = q(t) - \bar{q}(t)$, apply Eqs. (15, 16 and 17) and then add and subtract $B_0F_0\varepsilon(t)$ we obtain

$$\dot{\varepsilon}(t) = (R + B_0F_0)\varepsilon(t) + Q^{-1}(t)B(t)u_t(t) - B_0F_0q(t). \tag{18}$$

If we choose the appropriate matrix F_0, the stability matrix (Eq. 18) is $(R + B_0F_0)$, and, therefore, the systems (Eq. 15) and (Eq. 16) will be considered equivalent if

$$Q^{-1}(t)B(t)u_t(t) = B_0F_0q(t), \text{for all } t \geq 0, \tag{19}$$

and, therefore,

$$u_t(t) = B^*(t)Q(t)B_0F_0q(t), \text{where } B^* = (B^TB)^{-1}B^T. \tag{20}$$

By applying to Eq. (20) the inverse Lyapunov-Floquet transformation $q(t) = Q^{-1}(t)z(t)$ we obtain

$$u_t(t) = B^*(t)Q(t)B_0F_0Q^{-1}(t)z(t),$$

and, therefore, we conclude that the time-varying gain matrix $F(t)$ is given by

$$F(t) = B^*(t)Q(t)B_0F_0Q^{-1}(t).$$

Therefore, the state-feedback control law can be expressed as

$$u_t = -B^*(t)Q(t)B_0F_0Q^{-1}(t)z(t), \tag{21}$$

Analytical model of the energy harvesting mechanism

Vibrational energy harvesting structures encompass a range of configurations, with cantilevered beams or plates being the most prevalent. These typically feature partial or full coverage with a piezoelectric (PZT) layer (Challa et al., 2008 and Zhu, 2011). The structure examined in this study consists of a free-floating beam partially coated with a piezoelectric material layer and subjected to parametric excitation, as depicted in Figure 2.

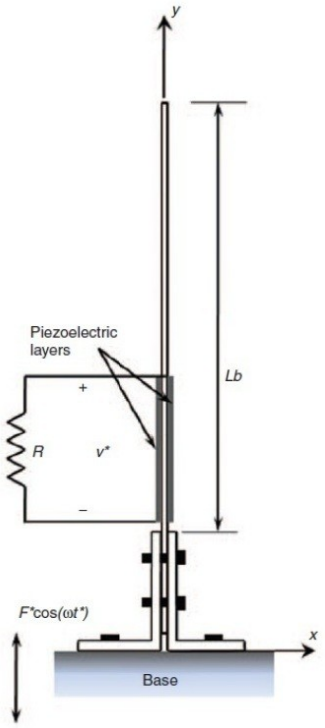

Figure 2. Proposed Collector Model (Daqaq et. al., 2009).

The piezoelectric material is connected to the beam and a resistive load for energy harvesting. The mathematical model representing these dynamics was described by Daqaq et al (2009), whose dynamic equations are given by Eq. (22)

$$\begin{cases} \ddot{u} + 2\mu_1\dot{u} + \omega_n^2 u + \mu_2|\dot{u}|\dot{u} + \alpha u^3 + 2\beta(u^2\ddot{u} + u\dot{u}^2) = u\frac{F}{m}\cos(\omega t) + \frac{\theta}{m}V, \\ \theta\dot{u} + C_p\dot{V} + \frac{1}{R}V = 0, \end{cases} \tag{22}$$

where u is the generalized coordinate representing the deflection of the beam in the x direction, V is the output voltage measured at the resistor R, μ_1 is the viscous damping term, μ_2 is the quadratic damping representing the air resistance, α and β are constants, θ is the electromechanical coupling, C_p is the capacitance of the piezoelectric element, m is the mass of the beam, F is the excitation amplitude, and ω is the excitation frequency. The term αu^3 is used to describe the geometric nonlinearity of the beam, the term $2\beta(u^2\ddot{u} + u\dot{u}^2)$ represent the inertia. The deflection of the beam, u, nd the time, t, are normalized with respect to its length, Lb, and the inverse frequency response, $\frac{1}{\omega_n}$, respectively. After normalization, the equivalent system given in Eq. (23) is obtained

$$\begin{cases} \ddot{x} + 2\mu_1\dot{x} + x + \mu_2|\dot{x}|\dot{x} + \alpha x^3 + 2\beta(x^2\ddot{x} + x\dot{x}^2) = xF\cos(\Omega t) + \frac{\theta}{K}V, \\ \theta\dot{x} + C_p\dot{V} + \frac{1}{R_{eq}}V = 0, \end{cases} \tag{23}$$

where $x = \frac{u}{Lb}$, $t = t\omega$, $V = \frac{V}{Lb}$, $\mu_1 = \frac{\mu_1}{\omega_n}$, $\mu_2 = \mu_2 Lb$, $\alpha = \alpha\frac{Lb^2}{\omega_n^2}$, $\beta = \beta(Lb)^2$, $F = \frac{F}{K}$, $C_p = C_p$, $R_{eq} = R\omega_n$, $\Omega = \frac{\omega}{\omega_n}$, $K = m\omega_n^2$.

The time-averaged output power generated by the system described in Eq. (23), over a time interval of length h, is defined as

$$P = \frac{1}{h}\int_{t_0}^{t_0+h} \lambda V(t)^2 dt \tag{24}$$

where $\lambda V(t)^2$ is the instantaneous power and $\lambda = \frac{1}{R_{eq}C_p}$ (Norenberg et al., 2022).

Results and discussions

In the numerical analyses conducted throughout this study, the model parameters received the following nominal values: $\mu_1 = 0.01$, $\mu_2 = 0.01$, $\alpha = 0.001$, $\beta = 0.001$, $K = 0.5$, and $R_{eq} = 20$. Several values were considered for the parameters F, Ω, and C_p, representing, respectively, the amplitude and frequency of the applied parametric excitation, as well as the capacitance of the piezoelectric component. All computational simulations were performed using MATLAB software (version R2022a, MathWorks Inc.). The initial conditions were defined by the state vector (x_0, $\dot{x}_0$, V_0) = (0.1, 0.0).

Stability and global sensitivity analysis

Initially, the numerical results for the stability analysis based on the Floquet method (Meirovitch, 2010; Monteiro, 2011; Naifeh & Balachandran, 1995) and a state transition matrix approximation technique (Sinha & Butcher, 1997) are presented.

For the global sensitivity analysis, the physical parameters of the system were assumed to be independent, and a uniform distribution over their nominal values was adopted with a coefficient of variation of up to 20%.

Stability analysis

To analyze the dynamic stability of the system and identify potential steady-state solutions, the dimensionless dynamic equations (Eq. (23)) are reformulated into a set of state-space equations. For this purpose, we introduced the change of variable $x_1 = x$, $x_2 = \dot{x}$, $x_3 = V$, and obtained the state-space representation of the system is formulated as follows

$$\begin{cases} \dot{x}_1 = x_2 = f_1(x,t) \\ \dot{x}_2 = \frac{1}{1+2\beta x_1^2}\left[-2\mu_1 x_2 - x_1 - \mu_2|x_2|x_2 - \alpha x_1^3 - 2\beta x_1 x_2^2 + x_1 F\cos(\Omega t) + \frac{\theta}{K}x_3\right] = f_2(x,t) \\ \dot{x}_3 = -\frac{\theta}{C_p}x_2 - \frac{1}{C_p R_{eq}}x_3 = f_3(x,t) \end{cases} \tag{25}$$

The system has three equilibrium points (x_1^*, x_2^*, x_3^*), namely $(0,0,0)$, $\left(\sqrt{\frac{F-1}{\alpha}}, 0, 0\right)$, $\left(-\sqrt{\frac{F-1}{\alpha}}, 0, 0\right)$. The last two equilibrium points are valid only when $\Omega = 0$, i.e., the system is free from periodic excitation. This paper considers only the system (Eq. (23)) under periodic forcing; consequently, the analysis is focused exclusively on the equilibrium point $(0,0,0)$.

To implement Sinha's method (Sinha and Butcher, 1997), it is necessary to linearize the equations of states (Eq. (25)) around the equilibrium point $(0,0,0)$. Thus, the equations of the system can be written in the form $\dot{x}(t,\mathcal{P}) = A(t,\mathcal{P})x(t,\mathcal{P})$, where $\mathcal{P}$ represents its parameters, and $A(t,\mathcal{P})$ is a periodic matrix of period $T = \frac{2\pi}{\Omega}$. By performing the transformation $t = \frac{2\pi}{\Omega}\tau$, the linearized system is rewritten in the form $\frac{dx}{d\tau} = \bar{A}(\tau,\mathcal{P})x(\tau,\mathcal{P})$ where $\bar{A}(\tau,\mathcal{P}) = \bar{A}_1(\mathcal{P})f_1(\tau) + \bar{A}_2(\mathcal{P})f_2(\tau)$, $f_1(\tau) = 1$, $f_2(\tau) = \cos(2\pi\tau)$,

$$\bar{A}_1(\mathcal{P}) = \frac{2\pi}{\Omega}\begin{bmatrix} 0 & 1 & 0 \\ -1 & -2\mu_1 & \frac{\theta}{K} \\ 0 & -\frac{\theta}{C_p} & -\frac{1}{C_p R_{eq}} \end{bmatrix}, \bar{A}_2(\mathcal{P}) = \frac{2\pi}{\Omega}\begin{bmatrix} 0 & 0 & 0 \\ F & 0 & 0 \\ 0 & 0 & 0 \end{bmatrix}.$$

To analyze the structural stability, we investigated whether the modulus of the characteristic multipliers ρ_j is greater than or equal to 1 for given values of the physical parameters. These multipliers can be calculated by the Approximate Fundamental Matrix. In the approximation, the degree of the modified Chebyshev polynomial is $m = 20$, and the number of Picard iterations is $p = 40$. In the stability analysis, the nominal value of the electromechanical coupling coefficient was set to $\theta = 0.1$.

Figures 3a through 3d present the stability charts associated with the equilibrium point (0,0,0), considering variations in the amplitude of the external excitation force F. In these diagrams, the dashed line serves solely as a visual reference to indicate the threshold modules of the characteristic multipliers. The equilibrium is classified as asymptotically stable whenever all characteristic multipliers have moduli below this reference line. Conversely, when any of the moduli exceed this threshold, the equilibrium point becomes unstable. In Figure 3*a*, $\Omega = 0.9$ was adopted and the amplitude F was varied in the interval $[0.01, 1]$. There is a range of values of F for which the equilibrium point of the system is stable, i.e., the characteristic multipliers have modulus less than 1, and a condition for instability in the range of values in which the multipliers have modulus greater than 1. Figure 3*b* presents the stability diagram in the resonance region $1:1$ ($\Omega = 1$). The stability change occurs for smaller values of the amplitude F than what occurs for $\Omega = 0.9$. Figure 3*c* shows the stability diagram for the system under the $2:1$ internal resonance condition ($\Omega = 2$). In this case, a transition in stability is observed within a narrow range of the excitation amplitude, specifically for $F \in [0.001, 0.08]$. In Figure 3*d*, the parameters are set to $\Omega = 0.64$ with $0.01 \leq F \leq 0.9$. It is again observed that the system exhibits both stable and unstable regions, as the characteristic multipliers lie within the unit circle for certain values of F, indicating stability, while for other values they lie outside the unit circle, indicating instability.

Figure 3*e* illustrates the regions of stability (shaded in blue) and instability (shaded in green) in the $\Omega - F$ parameter space. The blue area corresponds to combinations of Ω and F for which all characteristic multipliers have a modulus less than one, indicating stable behavior. Conversely, the green area identifies regions where at least one multiplier has a modulus greater than one, signaling instability. The stability profiles observed in Figures 3a through 3d are consistent with the regions highlighted in Figure 3*e*. Within the stability region, the system trajectories converge to the equilibrium point at $(0,0,0)$. As an example, for $F = 0.1$ and $\Omega = 1.6$, the moduli of the characteristic multipliers are $|\rho_1| = |\rho_2| = 0.9615$ and $|\rho_3| = 0.9902$, confirming stable dynamics. In contrast, for $F = 0.0565$ and $\Omega = 2$, the values $|\rho_1| = 1.013$, $|\rho_2| = 0.927$, and $|\rho_3| = 0.9922$ indicate that the system is unstable due to one multiplier exceeding unity in magnitude.

To further investigate the system's behavior under specific conditions, time-domain simulations of the beam displacement were carried out, as presented in Figure 4. Figures 4a and 4b depict two distinct dynamic responses corresponding to different parameter combinations.

In Figure 4a, the excitation parameters are set to $F = 0.1$ and $\Omega = 1.6$, corresponding to a stable configuration within the identified stability region. Under these conditions, the system response asymptotically converges to the equilibrium position. Figure 4b illustrates the case $F = 0.0565$, and $\Omega = 2$, which falls within the instability region, as previously determined through the analysis of characteristic multipliers. In this case, the system exhibits an initial transient phase followed by a transition into a periodic

regime. Figure 4c provides a detailed view of the system's response over the time interval $[7800, 8000]$, accompanied by the associated Poincaré sections, offering further insight into the long-term dynamical behavior.

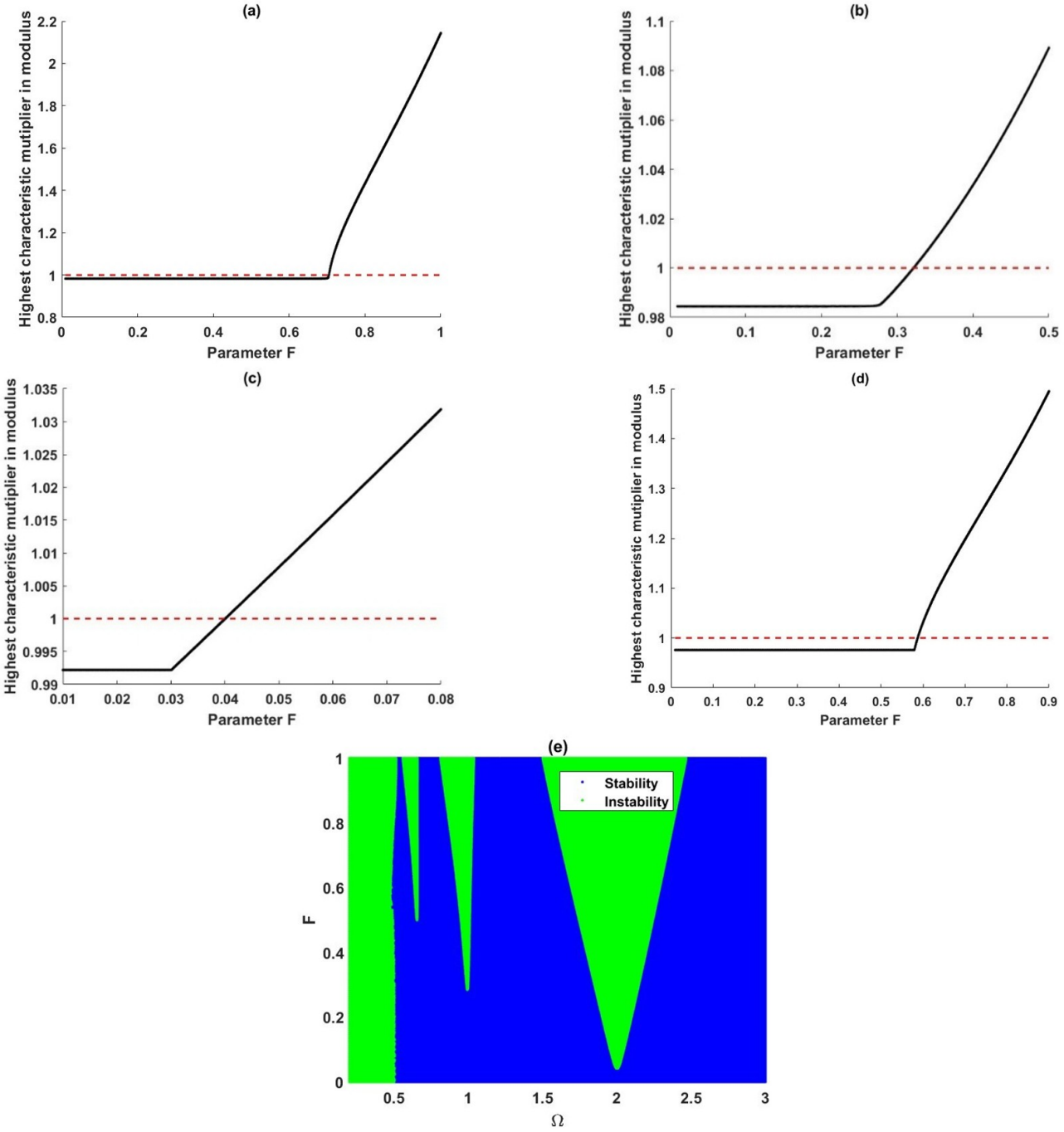

Figure 3. (*a*) Stability diagram for $\Omega = 0.9$, (*b*) Stability diagram for $\Omega = 1$, (*c*) Stability diagram for $\Omega = 2$, (*d*) Stability diagram for $\Omega = 0.64$, (*e*) Stability region: $0.01 \leq \Omega \leq 3.0$, and $0.01 \leq F \leq 1$.

To start a global sensitivity analysis, the first step is to verify that the surrogate model is a good approximation to the original model of the problem. The surrogate model used in this study is based on the Polynomial Chaos Expansion of the average power produced by the energy harvester, which aims to measure the relative importance of each parameter of the system in energy production. In order to validate the surrogate model, we adopted $C_p = 20$ and the following values for the parametric power parameters: $F = 0.28$ and $\Omega = 0.65$. Unless otherwise specified, whenever we set a nominal value for a parameter, it will be allowed to vary by up to 20%. In Figure 5, a correlation is made between the data generated by the original model (True Model) and the data of the surrogate model (Surrogate Model). Figure 5 shows that the surrogate model is a good approximation to the true model since their data closely follow the identity curve.

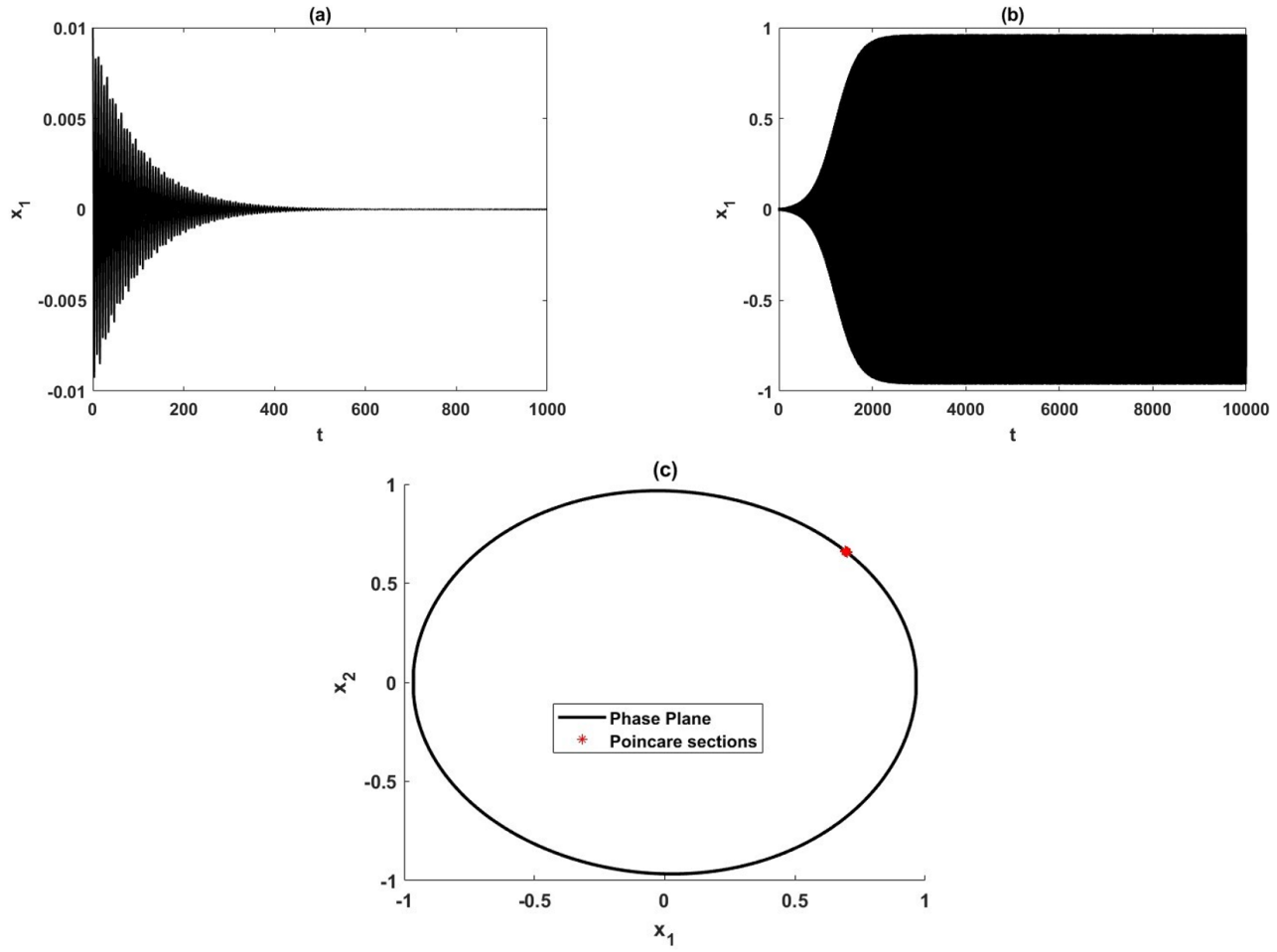

Figure 4. Time history for the displacement of the beam: (a) $F = 0.1$ and $\Omega = 1.6$, (b) $F = 0.0565$ and $\Omega = 2$, (c) Phase space and Poincaré section for $F = 0.0565$ and $\Omega = 2$.

Global sensitivity analysis

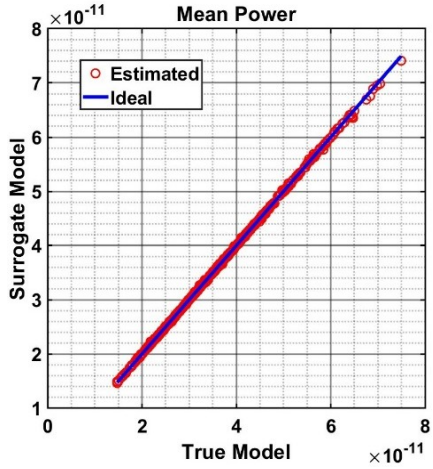

Figure 5. Average power P: comparison between surrogate model and true model.

These results allow us to explore, using the surrogate model, scenarios that can significantly influence the average output power P (Eq. (24)) of the energy harvester. Figure 6a shows the global sensitivity analysis via Sobol indices for the energy collector, in order to analyze the influence of the parameters on the average output power. In this section, special attention has been given to the analysis of the resonance regions, and this is due to the possibility of the system being driven into a periodic regime for small values of the amplitude of the parametric force F (Figure 3e). For energy production, the equilibrium point is expected not to have asymptotic stability, i.e., that the system operates in a region of instability, in a periodic regime.

For Ω ranging from 0.6 to 0.66, and $F = 0.82$, the frequency Ω, and the amplitude F, followed by the capacitance C_p, are parameters associated with the highest sensitivity. In Figure 6b, $F = 0.7$ and Ω ranging from 0.9 to 1.02 were adopted. It is important to highlight that the values of Ω were selected to enable analysis of the system in the vicinity of the primary resonance condition, specifically $\Omega = 1$, corresponding to the $1:1$ resonance. Under this condition, the system exhibits increased sensitivity to variations in the excitation frequency Ω, followed by the excitation amplitude F, and subsequently by the capacitance C_p. Figure 6c shows an analysis of the system around the resonance region $2:1$ ($\Omega = 2$) with a variation of 20%, i.e., Ω ranging from 1.8 to 2.2 and assuming $F = 0.4$. In this condition, there was an increase in the importance of capacitance C_p in the average power generated by the energy collector. So, the system is most sensitive to the amplitude F, then the capacitance C_p, and at last the frequency Ω. We conclude, from Figures 6a, 6b, and 6c, and respectively from the imposed conditions, that the frequency and amplitude of the parametric force, as well as the capacitance of the piezoelectric element, are associated with the highest sensitivity, meaning that they are the parameters that most affect the behavior of the system.

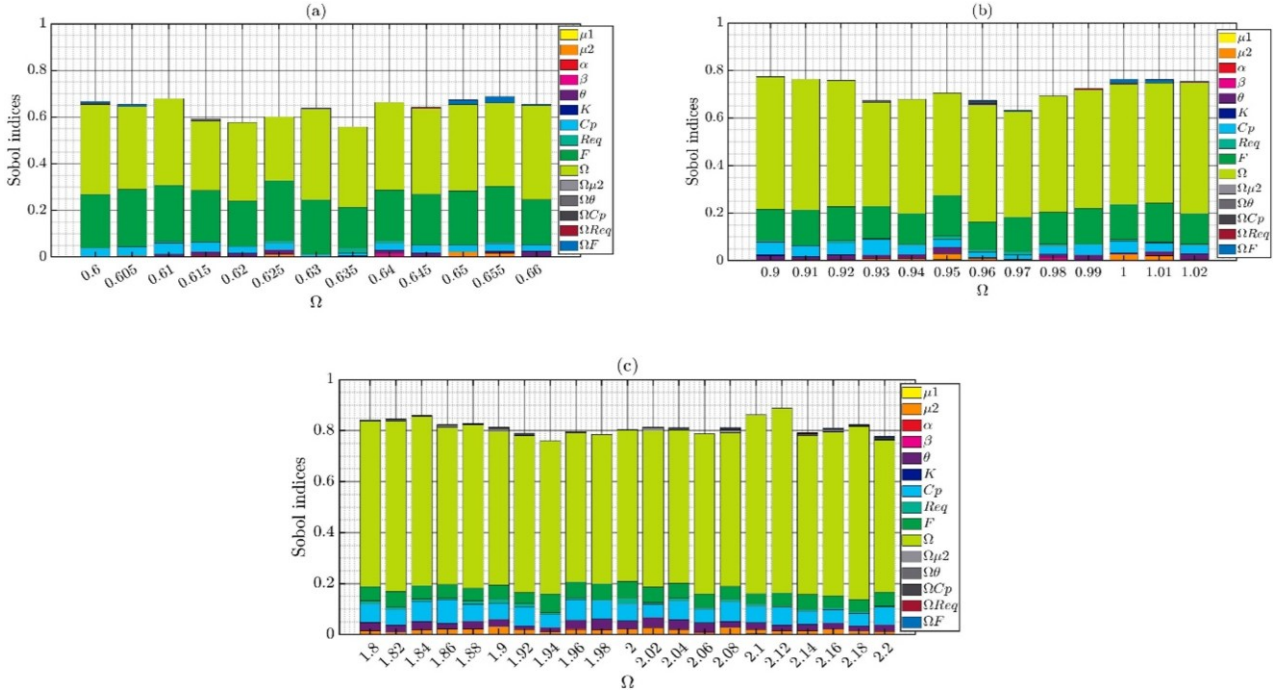

Figure 6. (a) Sobol indices for $0.6 \leq \Omega \leq 0.66$, $F = 0.82$ and $\theta = 0.05$; (b) Sobol indices for $0.9 \leq \Omega \leq 1.02$, $F = 0.7$ and $\theta = 0.05$; (c) Sobol indices for $1.8 \leq \Omega \leq 2.2$, $F = 0.4$ *and* $\theta = 0.05$.

In Figure 7, the sensitivity of the system was evaluated in the resonance regions: $\Omega = 1.0$ (Figure 7a) and $\Omega = 2.0$ (Figure 7b). For Figure 7a, in turn, F ranges from 0.28 and 0.88 with a step size of 0.04. At last, in Figure 7b F ranges from 0.06 to 0.2 with a step size of 0.01.

Figure 7a shows the predominance of Ω in most scenarios followed by the amplitude F. The contribution of capacitance C_p also increases when increasing the amplitude F. In Figure 7b, we observe behaviors similar to those of Figure 7a, that is, a greater relative contribution in the energy production of parameters Ω, F, and C_p.

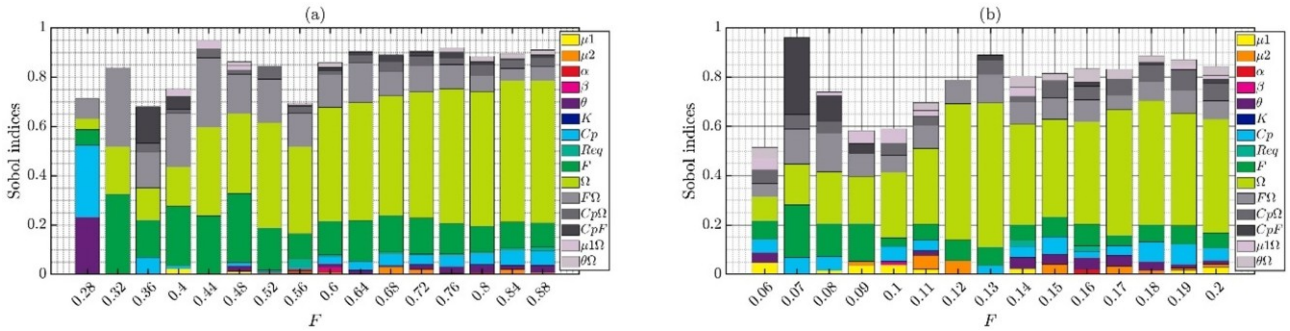

Figure 7. (a) Sobol indices for $0.28 \leq F \leq 0.88$, $\Omega = 0.82$ and $\theta = 0.05$; (b) Sobol indices for $0.06 \leq F \leq 0.2$, $\Omega = 2$ and $\theta = 0.05$.

Taking into account the stability region (Figure 3e) and the sensitivity of the average output power of the system to parameters Ω and C_p in the neighborhood of $\Omega = 2$ (Figure 6c), the time histories of the displacement x_1 (Figure 8a) and the voltage x_3 (Figure 8b) are presented. The system enters a periodic regime, as can be observed in the Poincaré section (Figure 9a) and the Lyapunov exponents (Figure 9b).

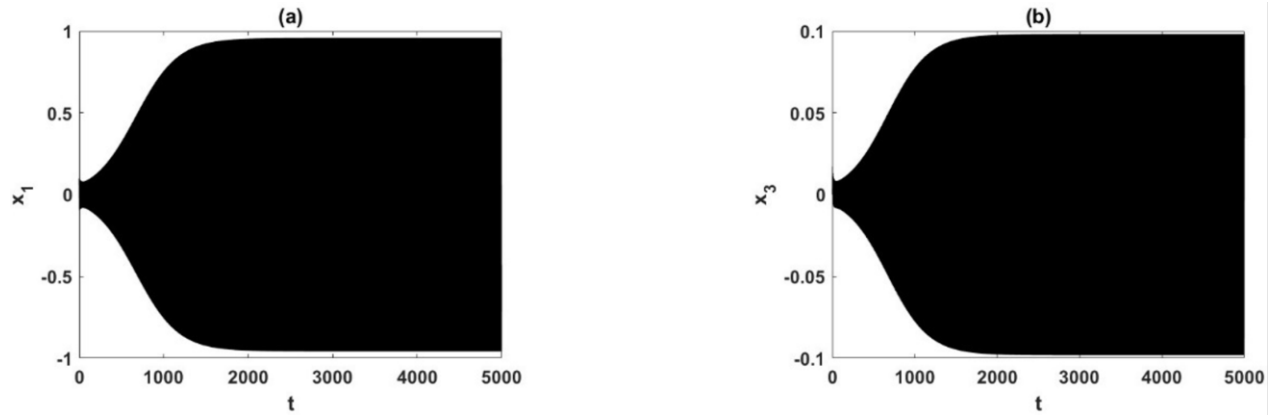

Figure 8. Response of the system for $F = 0.062$, $\Omega = 2$, $C_p = 2$, and $\theta = 0.05$.

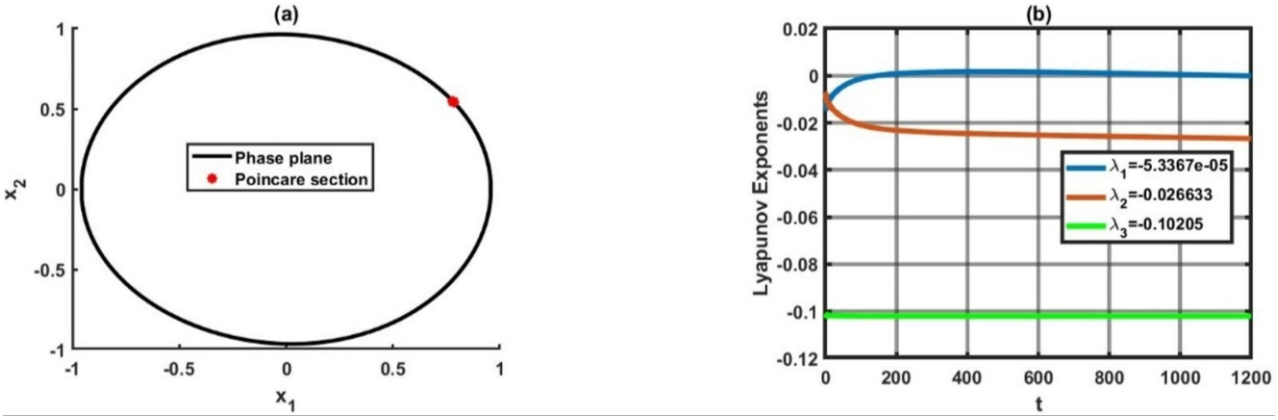

Figure 9. (a) Phase plane and Poincaré section; (b) Lyapunov exponents.

Figures 10a and 10b present the variation of the output mean power as a function of the capacitance C_p. The average output power was obtained through a polynomial approximation known in the literature as Polynomial Chaos Kriging (PCK) (Gaussian modeling process). Polynomial Chaos Kriging is a new metamodeling technique that combines Gaussian process modeling and Polynomial Chaos Expansion (Sudret, 2008). These results were obtained in the 2 : 1 resonance region, for values of Ω and F such that the system is close to the stability frontier, as shown in Figure 3e. Figure 10a shows the average power for $0 \leq C_p \leq 10$, while Figure 10b shows the magnification of Figure 10a for $0 \leq C_p \leq 2$. Peak power output is observed at approximately $C_p \approx 0.485$.

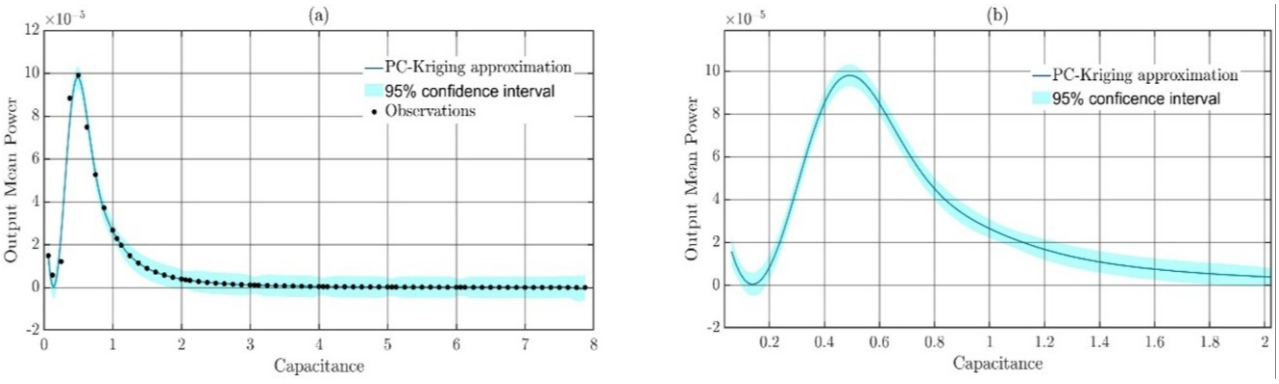

Figure 10. Output Mean Power via PC-Kriging approximation.

Control design using the lyapunov-floquet approach

This section aims to develop a control strategy capable of steering the open-loop system towards a predefined reference trajectory y. To this end, we chose the following parameter values: $\Omega = 2$, $F = 0.062$, $C_p = 0.485$, and $\theta = 0.05$. The choice of Ω and F was made following the stability studies of section 4.1.1 (Figure 3*e*). Under this condition, the equilibrium point $(0, 0, 0)$ of the system is unstable, but it enters the periodic regime (Figures 8 and 9.) The choice of the capacitance value C_p is derived from the global sensitivity analysis, for which the uncontrolled system presents a maximum in energy production (Figure 10).

Consider the nonlinear system (Eq. (25) rewritten as

$$\dot{x} = f(x,t) + u_c(t) \tag{26}$$

where $u_c(t)$ is the control law as described in Eq. (11), $x = (x_1, x_2, x_3)^T$ and $f(x,t) = (f_1(x,t), f_2(x,t), f_3(x,t))^T$ as in Eq. (25).

At each time instant t, define the error vector $e(t) = x(t) - y(t)$ where $x(t)$ denotes the state trajectory of the controlled system (Eq. (26)) and $y(t) = (y_1, y_2, y_3)^T$ represents the desired reference trajectory. Using this definition, the system in Eq. (26) can be reformulated in terms of the error dynamics $\dot{e} = g(e(t), t) + B(t)u(t)$.

By linearizing $g(e(t), t)$ around $e = 0$ and by carefully selecting the trajectory y as $y_1 = a + \varepsilon\cos(\Omega t)$, $y_2 = b + \varepsilon d\sin(\Omega t)$, $y_3 = c\cos(\Omega t)$, such that $a, b, c, d, \varepsilon \in \mathbb{R}$ are constant with $a > 0, b > 0, c > 0, d \neq 0, b > \varepsilon|d|$ and $0 < \varepsilon \ll 1$, we get

$$\dot{e} = A(t)e(t) + B(t)u(t) + G(e(t), \varepsilon), \tag{27}$$

where $G(e(t), \varepsilon)$ denotes the components related to power terms of ε,

$$A(t) = \begin{bmatrix} A_{11}(t) & A_{12}(t) & A_{13}(t) \\ A_{21}(t) & A_{22}(t) & A_{23}(t) \\ A_{31}(t) & A_{32}(t) & A_{33}(t) \end{bmatrix},\ A_{ij}(t) = \frac{\partial g_i}{\partial e_j}, A_{11}(t) = 0, A_{12}(t) = 1, A_{13}(t) = 0,$$

$$A_{21}(t) = -\frac{4\beta a}{(1+2\beta a^2)^2}[-2\mu_1 b - a - \mu_2 b^2 - \alpha a^3 - 2\beta a b^2] + \frac{1}{1+2\beta a^2}[-1 - 3\alpha a^2 - 2\beta b^2] - \left[\frac{4\beta a}{(1+2\beta a^2)^2}\left(aF + \frac{\theta}{K}c\right) - \frac{F}{1+2\beta a^2}\right]\cos(\Omega t),$$

$$A_{22}(t) = \frac{1}{1+2\beta a^2}[-2\mu_1 - 2\mu_2 - 4\beta a b], A_{23}(t) = \frac{\theta}{K(1+2\beta a^2)}, A_{31}(t) = 0, A_{32}(t) = -\frac{\theta}{C_p}$$

$$A_{33}(t) = -\frac{1}{C_p R_{eq}}$$

The system (Eq. (27)) is rewritten by parameterizing time $t = T\tau$, with $T = \frac{2\pi}{\Omega}$ as

$$\frac{d}{d\tau}e = \bar{A}(\tau)e(\tau) + B(\tau)u(\tau) + G(e(\tau), \varepsilon) \tag{28}$$

where $\bar{A}(\tau) = \bar{A}(\tau, \Lambda) = \bar{A}_1(\Lambda)f_1(\tau) + \bar{A}_2(\Lambda)f_2(\tau)$, $f_1(\tau) = 1$, $f_2(\tau) = \cos 2\pi\tau$,

$$\bar{A}_1(\Lambda) = \begin{pmatrix} 0 & 1 & 0 \\ \Theta_{21} & \Theta_{22} & \Theta_{23} \\ 0 & -\frac{\theta}{C_p} & -\frac{1}{C_p R_{eq}} \end{pmatrix},\ \bar{A}_2(\Lambda) = \begin{pmatrix} 0 & 0 & 0 \\ \Gamma & 0 & 0 \\ 0 & 0 & 0 \end{pmatrix},$$

$$\Theta_{21} = -\frac{4\beta a}{(1+2\beta a^2)^2}[-2\mu_1 b - a - \mu_2 b^2 - \alpha a^3 - 2\beta a b^2] + \frac{1}{1+2\beta a^2}[-1 - 3\alpha a^2 - 2\beta b^2],$$

$$\Theta_{22} = \frac{1}{1+2\beta a^2}[-2\mu_1 - 2\mu_2 - 4\beta a b], \Theta_{23} = \frac{\theta}{K(1+2\beta a^2)}, \Gamma = -\left[\frac{4\beta a}{(1+2\beta a^2)^2}\left(aF + \frac{\theta}{K}c\right) - \frac{F}{1+2\beta a^2}\right].$$

By applying the Lyapunov-Floquet transformation $e = Q(t)q$, Sinha's techniques for state transition matrix approximation, and using Eq. (28), we can rewrite the system (Eq. (27)) in the form

$$\dot{q} = Rq(t) + Q^{-1}(t)\bar{B}(t)u_t \tag{29}$$

in which

$$R = \begin{bmatrix} -0.0122 & 0.0203 & -0.0085 \\ 0.0104 & -0.0118 & -0.0001 \\ -0.0093 & -0.0030 & -0.1012 \end{bmatrix}.$$

The eigenvalues derived from the system's stability matrix (Eq. (29)) are $\lambda_1 = 0.0030$, $\lambda_2 = -0.0261$, and $\lambda_3 = -0.1020$. Since $\lambda_1 = 0.0030$, the time-invariant system (Eq. (29)) is unstable. Since the gain matrix of the system (Eq. (29)) is constant with respect to time, an equivalent time-invariant formulation of the system (Eq. (16)) must exist, along with a matrix B_0 that fulfills the conditions specified in Eqs. (16) to (19). In this work, B_0 is selected as I_3, the 3×3 identity matrix.

Based on the methodology outlined in the works of Sinha and Joseph (1994), David and Sinha (2000), and Sinha and Dávid (2006), a linear controller can be synthesized using the pole placement technique. By selecting the desired closed-loop poles at -1, -1, and -1, the resulting time-invariant gain matrix F_0, obtained through this procedure, is denoted by

$$F_0 = \begin{bmatrix} 0.9878 & 0.0203 & -0.0085 \\ 0.0104 & 0.9882 & -0.0001 \\ -0.0093 & -0.0030 & 0.8988 \end{bmatrix}.$$

Consequently, the control law for the nonlinear system described in Eq. (26) adopts the structure presented in Eq. (21), where the matrix function $Q(t)$ is defined according to Theorem 1.

Figure (11) illustrates the temporal responses of both the controlled and uncontrolled systems. It is evident that the states of the controlled system rapidly converge to the designated trajectory (see Figs. 11a, 11b, and 11c). Furthermore, a marked increase in the oscillation amplitude of the x_3 voltage is observed in the controlled system relative to the uncontrolled case, which contributes positively to enhanced energy harvesting (Figure 11c).

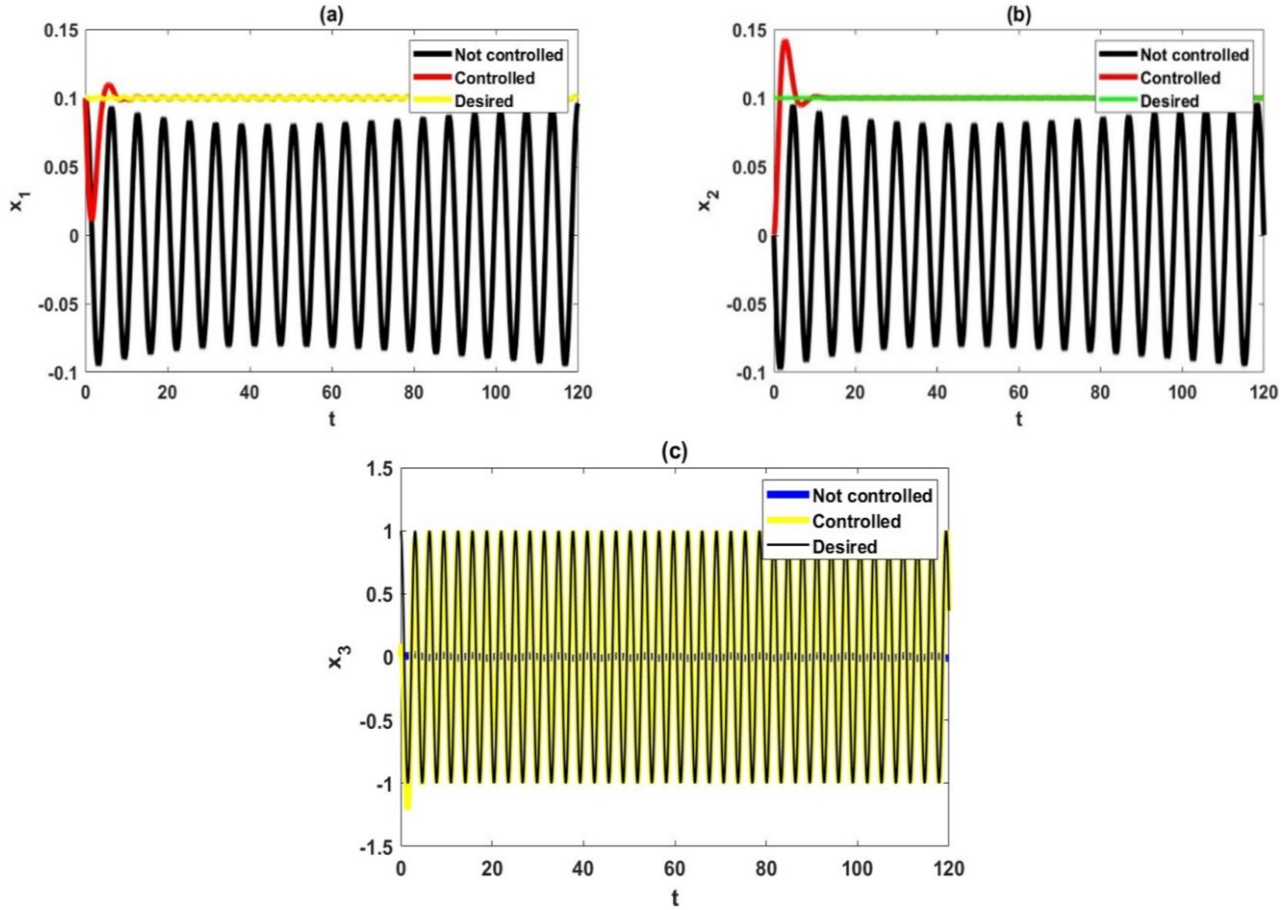

Figure 11. Time history of uncontrolled and controlled states: (a) Displacement of the beam x_1; (b) Velocity of the beam x_2; (c) Voltage x_3.

Figures 12a and 12b show the average power as a function of capacitance C_p for $0.05 \leq C_p \leq 1$. Figure 12a presents a comparison of the average power output between the controlled and uncontrolled systems. To provide greater detail, Figure 12b offers a magnified view of the region surrounding the curve corresponding to the average power of the uncontrolled system.

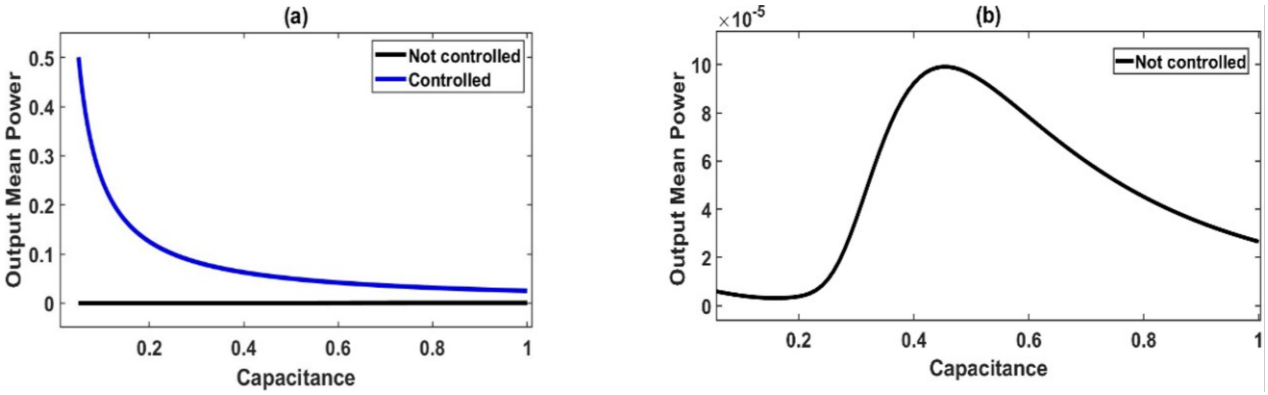

Figure 12. Output Mean Power: (a) Controlled vs. uncontrolled system comparison; (b) Zoomed-in view of (a) focusing on the uncontrolled response.

Conclusion

The stability analysis conducted in this study revealed that the equilibrium point of the system may exhibit either stable or unstable behavior, contingent upon the selected nominal values of the parameters defining the parametric excitation. At the boundary separating the stable and unstable regions, periodic operating regimes were identified and explored.

The global sensitivity analysis via Sobol indices evidenced that near the resonance region, the most relevant parameter for energy harvesting is the frequency of the parametric force. Also, in the resonance region $2 : 1$, the system is sensitive to the capacitance variation.

The stability and sensitivity analyses offer complementary insights that contribute to the development of a more effective control strategy for energy harvesting in the system under investigation.

Ultimately, the controller designed based on the Lyapunov-Floquet transformation successfully guided the system's trajectory toward the desired reference. As a result, a substantial improvement in the system's energy output was achieved.

References

Andò, B., Baglio, S., Trigona, C., Dumas, N., Latorre, L., & Nouet, P. (2010). Nonlinear mechanism in MEMS devices for energy harvesting applications. *Journal of Micromechanics and Microengineering, 20*(12), 125020. https://doi.org/10.1088/0960-1317/20/12/125020

Andrade, E. X. L., Bracciali, C. F., & Rafaeli, F. R. (2012). *Introdução aos Polinômios Ortogonais*. Sociedade Brasileira de Matemática Aplicada e Computacional.

Bhat, L. A., Mishra, L. N., Mishra, V. N., Tunc, C., & Tunc, O. (2024). Precision and efficiency of an interpolation approach to weakly singular integral equations. *International Journal of Numerical Methods for Heat & Fluid Flow, 34*(3), 1479-1499. https://doi.org/10.1108/HFF-09-2023-0553

Butcher, E. A., & Sinha, S. C. (1998). Symbolic computation of local stability and bifurcation surfaces for nonlinear time-periodic systems. *Nonlinear Dynamics, 17*, 1-21. https://doi.org/10.1023/A:1008284325276

Cacuci, D. G. (2003). *Sensitivity and uncertainty analysis: Theory* (Vol. 1). Chapman & Hall/CRC.

Cauz, L. O., Chavarette, F. R., & Almeida, E. F. (2023). Global sensitivity and stability analysis of a parametrically excited energy harvesting system. *Journal of Vibration Testing and System Dynamics, 7*, 253-263. https://doi.org/10.5890/JVTSD.2023.09.001

Challa, V. R., Prasad, M. G., Shi, Y., & Fisher, F. T. (2008). A vibration energy harvesting device with bidirectional resonance frequency tunability. *Smart Materials and Structures, 17*(1), 015035. https://doi.org/10.1088/0964-1726/17/01/015035

Daqaq, M. F., Stabler, C., Qaroush, Y., & Seuaciuc-Osório, T. (2009). Investigation of power harvesting via parametric excitations. *Journal of Intelligent Material Systems and Structures, 20*, 545-557. https://doi.org/10.1177/1045389X08100978

David, A., & Sinha, S. C. (2000, June). Control of chaos in nonlinear systems with time-periodic coefficients. In *Proceedings of the American Control Conference* (pp. 764–768). IEEE.

Eichhorn, C., Goldschmidtboeing, F., Porro, Y., & Woias, P. (2009r). A piezoelectric harvester with an integrated frequency-tuning mechanism. In *Proceedings of Power MEMS 2009* (pp. 45–48). https://www.researchgate.net/publication/228514136

Iakubovich, V. A., & Starzhinskii, V. M. (1975). *Linear differential equations with periodic coefficients*. John Wiley.

Meirovitch, L. (1970). *Methods of Analytical Dynamics*. McGraw-Hill.

Meirovitch, L. (2010). *Methods of Analytical Dynamics*. Courier Corporation.

Monteiro, L. H. A. (2011). *Sistemas Dinâmicos*. Editora Livraria da Física.

Naifeh, A. H., & Balachandran, B. (1995). *Applied Nonlinear Dynamics*. John Wiley.

Norenberg, J. P., Cunha Jr, A., Silva, S., & Varoto, P. S. (2022). Global sensitivity analysis of asymmetric energy harvesters. *Nonlinear Dynamics, 109*(2), 443-458. https://doi.org/10.1007/s11071-022-07563-8

Outa, R., Chavarette, F. R., Gonçalves, A. C., da Silva, S. L., Mishra, V. N., Panosso, A. R., & Mishra, L. N. (2021). Reliability analysis using experimental statistical methods and AIS: application in continuous flow tubes of gaseous medium. *Acta Scientiarum. Technology, 43*(1), 1-19. https://doi.org/10.4025/actascitechnol.v43i1.55825

Rathour, L., Singh, V., Yadav, H., Sharma, M. K., & Mishra, V. N. (2024). A dual Hesitant Fuzzy set theoretic approach in Fuzzy reliability analysis of a Fuzzy system. *Inf. Sci. Lett., 13*(2), 433-440. https://doi.org/10.18576/isl/130219

Sharma, A., & Sinha, S. C. (2018). An approximate analysis of quasi-periodic systems via Floquet theory. *Journal of Computational and Nonlinear Dynamics, 13*, 1-18. https://doi.org/10.1115/1.4037797

Sharma, M. K., Dhiman, N., Kumar, S., Rathour, L., & Mishra, V. N. (2023). Neutrosophic Monte Carlo Simulation approach for decision making in medical diagnostic process under uncertain environment. *International Journal of Neutrosophic Science, 22*(1), 8-16. https://doi.org/10.54216/IJNS.220101

Sharma, M. K., Sadhna, C., Bhargava, A. K., Kumar, S., Rathour, L., Mishra, L. N., & Pandey, S. (2022). A fermatean fuzzy ranking function in optimization of intuitionistic fuzzy transportation problems. *Advanced Mathematical Models & Applications, 7*(2), 191-204.

Sinha, S. C., & Butcher, E. A. (1997). Symbolic computation of fundamental solution matrices for linear time-periodic dynamical systems. *Journal of Sound and Vibration, 206*, 61-85. https://doi.org/10.1006/jsvi.1997.1079

Sinha, S. C., & Dávid, A. (2006). Control of chaos in nonlinear systems with time-periodic coefficients. *Philosophical Transactions of the Royal Society A: Mathematical, Physical and Engineering Sciences, 364*, 2417-2432. https://doi.org/10.1098/rsta.2006.1832

Sinha, S. C., Henrichs, J. T., & Ravindra, B. (2000). A general approach in the design of active controllers for nonlinear systems exhibiting chaos. *International Journal of Bifurcation and Chaos, 10*, 165-178. https://doi.org/10.1142/S0218127400000104

Sinha, S. C., & Joseph, P. (1994). Control of general dynamic systems with periodically varying parameters via Liapunov-Floquet transformation. *ASME. Journal of Dynamic Systems, Measurement, and Control, 116*(4), 650-658. https://doi.org/10.1115/1.2899264

Soize, C. (2017). *Uncertainty Quantification: An Accelerated Course with Advanced Applications in Computational Engineering* (Vol. 1). Springer.

Sohn, J. W., Choi, S. B., & Lee, D. Y. (2005). An investigation on piezoelectric energy harvesting for MEMS power sources. *Proceedings of the Institution of Mechanical Engineers, Part C: Journal of Mechanical Engineering Science, 219*, 429-436. https://doi.org/10.1243/095440605X16947

Sudret, B. (2008). Global sensitivity analysis using polynomial chaos expansions. *Reliability Engineering & System Safety, 93*(7), 964–979. https://doi.org/10.1016/j.ress.2007.04.002

Zhu, D. (2011). Vibration energy harvesting: machinery vibration, human movement, and flow induced vibration. In *Sustainable Energy Harvesting Technologies-Past, Present and Future* (pp. 22–54). InTech. https://doi.org/10.5772/25731